Met. Mater. Int., Vol. 19, No. 4 (2013), pp. 731~740
doi: 10.1007/s12540-013-4012-8

Imitating Seasonal Temperature Fluctuations for the H_2S Corrosion of 304L and 316L Austenitic Stainless Steels

A. Davoodi[1,*], M. Babaiee[2], and M. Pakshir[3]

[1]Hakim Sabzevari University, Faculty of Engineering, Materials Science and Polymer Engineering Department, Sabzevar, 391, Iran
[2]Shiraz University, School of Engineering, Department of Materials Science and Engineering, Shiraz, 713451154, Iran
[3]Shiraz University, School of Engineering, Department of Materials Science and Engineering, Shiraz, 713451154, Iran

(received date: 6 January 2012 / accepted date: 3 September 2012)

Temperature fluctuations are inevitable in sour oil and gas production. In this study, the H_2S corrosion of 304L and 316L alloys was investigated at pH 3 and temperatures of 20-60 °C using DC and AC electrochemical techniques. Two-fold increases in the corrosion rates of both alloys were reported with increases in temperature to 60 °C. In the 304L alloy, the surface layer was observed to be 3% rougher and 34% thicker than that of the 316L alloy. The two alloys exhibited different corrosion behaviors in the temperature ranges of 20-40 °C and 40-60 °C. Although the 316L alloy revealed a greater corrosion resistance at the free potential condition, the passivation on the 304L alloy was significantly greater than that of the 316L alloy at 40 °C and 15 ppm H_2S. The FeS_2 and combined FeS_2-MoS_2 compounds contributed to the surface layer constituents in the 304L and 316L alloys, respectively. The increase in temperature kinetically provided more favorable conditions for FeS_2 than MoS_2 formation, i.e. it had a relatively constructive effect on the 304L alloy passivation.

Key words: alloys, corrosion, electrochemistry, microstructure, scanning electron microscopy (SEM), X-ray diffraction

1. INTRODUCTION

Stainless steel grades 304L and 316L are commonly used construction materials for piping, stationary, and rotary equipment that come in contact with corrosive environments during the production of hydrocarbon fluids [1,2]. Their corrosion resistance is attributed to the passive film formation on the alloy surface and the difference observed in the corrosion behavior of the 304L and 316L alloys has been associated with the additional molybdenum alloying element in the 316L alloy. It has been demonstrated that molybdenum participates in the surface reactions and enhances the protectiveness of the surface layer [3].

Nevertheless, the presence of hydrogen sulfide, carbon dioxide, dissolved salt, and water in the produced hydrocarbon fluids deteriorates the alloy passivity [4-6].The presence of the abovementioned contaminations becomes even more frequent as the exploitation of deep reservoirs increases and unconventional resources are increasingly used [2,7]. Despite several attempts to remove these contaminations [2,8-11], their presence is inevitable due to practical process restriction.

Among these impurities, the presence of hydrogen sulfide in produced oil and gas results in operational, environmental, and treatment problems. The procedure of selecting either the 304L or 316L alloy as the paramount alloy, from both an economical and performance viewpoint, is affected by the simultaneous influence of two kinetics parameters: the H_2S concentration and temperature [12]. High temperature H_2S corrosion on stainless steel has been reported recently and it was stated that the high concentration of sulfur in the sulfurated compounds favors the formation of extremely aggressive acids, such as H_2SO_4, which contribute to an accelerated and intense corrosion process of the stainless steel [13].

Three natural processes are proposed in order to explain the H_2S accumulations in the reservoirs: bacterial sulfate reduction (BSR), thermal cracking or thermal decomposition of sulfides (TDS), and thermochemical sulfate reduction (TSR) [7,14-17]. In addition, secondary H_2S could also be induced during the steam injection recovery process of heavy oil and gas [7]. In the southern Persian Gulf, the proposed TSR is a significant mechanism for obtaining high H_2S content, whereas the other processes, such as BSR and organic sulfur originated from the TDS of kerogen and/or oil, are also possible

*Corresponding author: adavoodi@kth.se

[16]. Hydrogen sulfide also changes the scaling tendencies of the construction materials [18-22]. Moreover, hydrogen sulfide and sour sulfur mass concentration affect the natural gas quality determination [23,24]. Sulfur components are soluble in sour gas and often precipitate during production if the temperature and pressure decrease, which lead to impairing the oil and gas well productivity and, consequently, the economics of reserve depletion [23].

The H_2S corrosion mechanism of various alloys is being investigated [25-28], but due to the high toxicity of the compound, the available experimental results are limited. However, laboratory-scale H_2S corrosion studies on some carbon steels with high safety facilities have been reported recently [29-31]. The results indicate that in the desired pH and immersion time, H_2S in acidic media increases the corrosion resistance of carbon steel compared with solutions without H_2S. This was attributed to the precipitation of a sulfide film, most likely mackinawite ($FeS_{(1-x)}$), cubic ferrous sulfide or pyrrhotite (FeS), troilite ($FeS_{(1+x)}$), and pyrite (FeS_2). In sequential papers, the H_2S corrosion on pure Fe, Cr, and Ni was studied in simulated experimental conditions with trace amounts of local H_2S produced by added Na_2S dissociation [32-35]. It was found that depending on the H_2S concentration, solution pH, and immersion time, H_2S could have an inhibiting or accelerating effect on the corrosion of pure Fe and Ni. However, for Cr, the corrosion rate generally increases with the presence of H_2S.

Electrochemical impedance spectroscopy (EIS) is effective for the characterization of the surface layers and identifying the H_2S corrosion mechanisms [12,31-32]. EIS is a nondestructive corrosion test in which a low amplitude AC potential signal in a desired frequency domain perturbs the alloy surface. The generated AC current is measured and the obtained impedance value (Z = V/I) as a complex variable is an indication of the alloy corrosion resistance [36]. An EIS study of H_2S corrosion on the 304L and 316L alloys in acidic media was recently conducted in which a lower corrosion rate was reported for the 316L alloy [12]. However, a higher passivation current density was observed during the anodic polarization on the 316L alloy, and the H_2S exhibited an inhibiting effect on the 304L alloy by decreasing the passivation current density [12].

In most oil and gas purification processes, temperature fluctuations are unavoidable due to process variables and seasonal climate changes. These fluctuations can have vital effects on the H_2S corrosion reactions, which indicate that in addition to the H_2S concentration, the temperature variations can affect the kinetics parameters, particularly the conditions for the surface layer formation. Despite its importance, a quantitative study of the influence of the temperature on the H_2S corrosion of 304L and 316L stainless steels in acidic media has not yet been conducted to accurately recognize its significance. This is a crucial task that will assist in determining whether the 304L alloy or the 316L alloy is more suitable for H_2S contaminated environments at various temperatures.

In this study, DC and AC electrochemical measurements including the open circuit potential (OCP) as a corrosion potential, the linear polarization resistance (LPR) as a corrosion resistance criterion, potentiodynamic polarization (PDP), and EIS tests were performed on 304L and 316L stainless steels in acidic media with 15 ppm of H_2S and at temperatures of 20, 40, and 60 °C. Comparisons between the experimental results and the multiple component Pourbaix diagrams of Fe, Ni, Cr, and Mo systems in the presence of sulfur components were also performed. X-ray diffraction (XRD) was used to characterize the sample surface morphologies and compositions after exposure to the H_2S corrosive media.

2. EXPERIMENTAL PROCEDURES

Analytical grade Na_2SO_4, Na_2S and H_2SO_4 reagents were used as corrosive media constituents. To prepare the solution, 1 M Na_2SO_4 solution was buffered by H_2SO_4 to a pH of 3. In order to exclusively investigate the H_2S corrosion mechanism and remove the dissolved oxygen, the solution was purged by an inert gas (Argon) for 15 min prior to each experiment. Then, the required amount of Na_2S, which produces 15 ppm (estimated from the following reaction in weight) H_2S, was added to the solution. According to the following reaction, Na_2S is dissociated to H_2S in acidic solutions [32-34,37,38]:

$$Na_2S + 2H^+ \rightarrow 2Na^+ + H_2S \quad (1)$$

As a result, a trace amount of H_2S was generated locally in the vicinity of the alloy surface. Argon purging and deoxygenating were continually applied during all measurements. A sealed electrochemical flat-cell (with 500 cm^3 in volume) was used and prior to adding Na_2S, the inert gas was purged into the solution (with flow rate of approximately 2 cm^3/s). After adding Na_2S (and producing H_2S), the argon was purged above (not into) the solution at a safe distance from the solution surface with the lowest possible pressure in order to avoid oxygen entering the solution. This could also avoid decreases in the H_2S concentration during the measuring time. Mounted cylindrical 304L and 316L austenitic stainless steel specimens with a diameter of1 cm were used as working electrodes. The chemical compositions of the alloys in wt% are given in Table 1. Prior to each experiment, the specimens were ground with 1200 SiC abrasive paper and then polished with 3 and 1 m alumina slurries to obtain mirror-like exposure surfaces.

The corrosion experiments were performed in the following sequence:

(a) 900 s OCP recording;

(b) LPR test with potential domain of ±10 mV and sweep rate of 0.5 mV/s;

Table 1. Chemical compositions of the 304L and 316L alloys used in this study

	C	S	P	Mo	Mn	Si	Cr	Ni	Fe
304L	0.02	0.02	0.03	0.30	1.62	0.46	18.13	8.7	Bal.
316L	0.02	0.02	0.02	2.30	1.71	0.49	18.16	8.2	Bal.

(c) Potentiostatic EIS test at OCP with an amplitude of 10 mV and a frequency range of 10^{-2}-10^{5} Hz; and,

(d) PDP test with a sweep rate of 1 mV/s and a potential range from -200 to 2000 mV with respect to OCP.

All measurements were taken three times to assure reproducibility. The corrosion tests were conducted using an Ivium Potentiostat instrument with saturated calomel and Pt wire as the reference and counter electrodes, respectively. The Ivium and EIS Spectrum Analyzer were used to extract the EIS equivalent circuit components. The simulated data was fitted with less than 1% error in calculation.

All measurements were performed in a water bath with controlled temperatures of 20, 40, and 60 ± 1 °C. These temperatures represent the actual seasonal temperature variations in Persian Gulf region. In order to identify the influence of the alloying elements, the experimental results were compared with multi-component Pourbaix diagrams of Fe-Ni-Cr (304L) and Fe-Ni-Cr-Mo (316L) aqueous systems and in the presence of H_2S species. All Pourbaix diagrams were plotted using Medusa software [39]. An equilibrium concentration of 10^{-6} M was used to dissolve the Fe, Ni, Cr, and Mo ions (i.e. $[Fe^{2+}(aq)] = [Cr^{3+}(aq)] = [Ni^{2+}(aq)] = [Mo^{4+}(aq)] = 10^{-6}$ M). It should be noted that in the Me-S-H_2O systems (where Me = Fe, Ni, Cr, and Mo), some other species, such as $FeCr_2O_4$, $NiFe_2O_4$, $NiCr_2O_4$, etc., may also exist that might not be considered due to their inactivity [40]. However, these compounds are most likely stable in neutral and alkaline conditions. Therefore, they do not have a significant contribution in the present study in acidic media.

Finally, scanning electron microscopy (SEM, Leica Cambridge, S360) and XRD (Bruker model D8 ADVANCE) was used to characterize the sample surface morphologies after exposure to the H_2S corrosive media.

3. RESULTS AND DISCUSSION

3.1. Corrosion potential

The corrosion potential variations are shown in Fig. 1. At all temperatures, the corrosion potential values associated with the 316L alloy were slightly more positive than those of the 304L alloy, which were approximately 10-20 mV. As seen in Fig. 1, increases in the temperature decrease both alloys' corrosion potentials. This is an indication of the increase in surface activity that is similar to the kinetics effect of the H_2S concentration [12]. In the previous study, it was found that increases in the H_2S concentration also decreased both alloys' corrosion potentials [12].

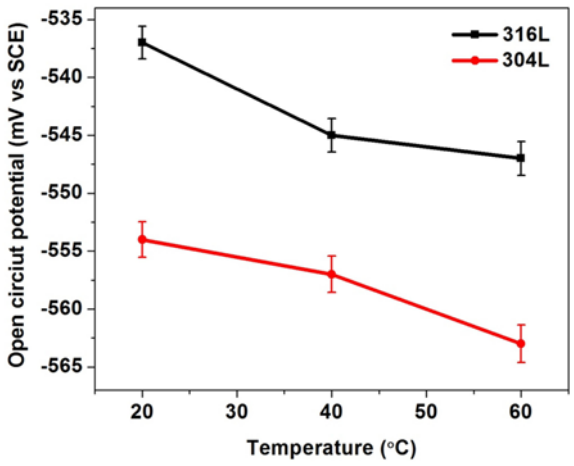

Fig. 1. Corrosion potential versus temperature in the 15 ppm H_2S solution.

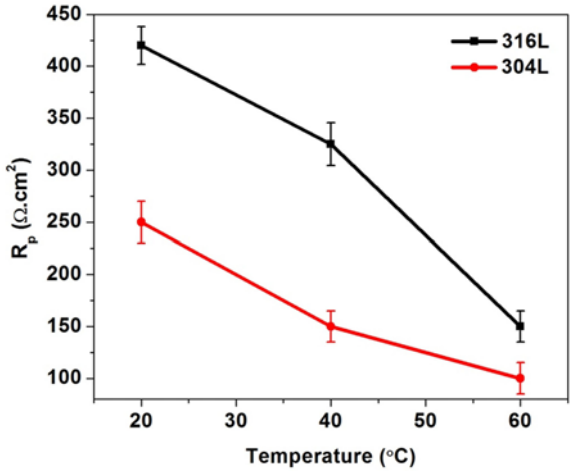

Fig. 2. Corrosion resistance (LPR, R_p) versus temperature in the 15 ppm H_2S solution.

3.2. LPR results

Figure 2 represents the influence of the temperature on the polarization resistance (R_p) value. At all temperatures, the R_p value of the 316L alloy was higher than that of the 304L alloy. The corrosiveness of the solution increases with increases in the temperature to 60 °C and the corrosion rate of both alloys increases. However, the influence of the temperature is more profound in the 316L alloy in which the R_p decreases to 150 Ω.cm^2 at 60 °C (i.e. a 250 Ω.cm^2 decrease). Apparently, the influence of the H_2S concentration on the corrosion rate is generally less important than the temperature variations [12]. This means that between these two process variables (H_2S

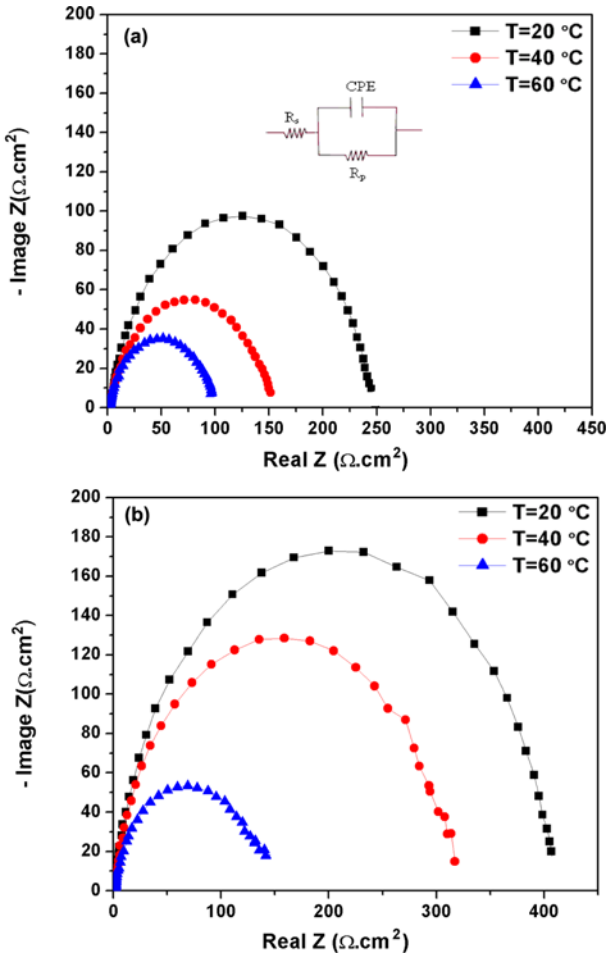

Fig. 3. EIS (Nyquist) plots of the (a) 304L and (b) 316L alloys at various temperatures in the 15 ppm H_2S solution. The inset presents the equivalent circuit used in the alloy-solution interface modeling.

concentration and temperature), the temperature has a greater influence on the corrosion rate. While increases in the H_2S concentration do not affect the R_p of the 304L alloy [12], increases in the temperature from 20 to 60 °C increase the corrosion rate at least 2.5 times.

3.3. EIS results

The EIS data can be presented in a Nyquist plot (imaginary versus real impedance). Figure 3 shows the Nyquist plots of the EIS results for the 304L and 316L alloys in a solution with 15 ppm H_2S at various temperatures. In all measurements, a single depressed capacitance loop containing one time constant could be observed. Comparing the Nyquist curves of the two alloys determined that at the same temperature, the semicircle diameter associated with the 316L alloy was larger than that of the 304L alloy. The alloy-electrolyte interface can be modeled using the equivalent circuit shown in the inset of Fig. 3, where R_s is the solution resistance, R_p is the polarization resistance at the alloy-electrolyte interface or charge transfer resistance, and CPE is a constant phase element. The CPE value can be expressed in the form of $Z_{CPE} = P^{-1}(j\omega)^{-n}$ in which P is related to the charge transfer capacitance (C_{ct}), j is complex number unit in which $j^2=-1$, n is a parameter related to the surface roughness and homogeneity, and ω is the angular frequency. Applying CPE, instead of pure capacitance, improves the fitness of the EIS data to the experimental results. Increases in the temperature do not induce other time constants; however, a decrease in the capacitance loop diameter and charge transfer resistance can be observed, which are indications of an increase in the corrosion rate.

The alloy-electrolyte interface parameters (R_s, R_p, n, and C_{ct}) can be extracted from the equivalent circuit shown in Table 2. The R_p values obtained from the EIS are very similar to those obtained from the LPR measurements. With increases in the temperature to 60 °C, the R_p of both alloys is reduced and the difference decreases. It appears that although the 316L alloy has a greater corrosion resistance at low temperatures, its superiority is diminished with temperature increases.

The charge transfer capacitance values can be calculated using the following equation [36,41]:

$$C_{ct} = (P(Rp)^{1-n})^{\frac{1}{n}} \quad (2)$$

The n and C_{ct} variations are shown in Fig. 4. Generally, the n value in the 316L alloy is smaller than that in the 304L alloy. In the 304L alloy, by increasing the temperature to 40 °C, the n value decreases rapidly from 0.87 to 0.80, and then slowly decreases to 0.78. In the 316L alloy, the n value decreased slightly from 0.90 to 0.87 with the increase in temperature to 40 °C and then more rapidly decreased to 0.81 at 60 °C. Decreases in the n value are indications of increases in the surface roughness and non-homogeneity that result from increases in the alloy surface dissolution in both alloys. Therefore, it can be concluded that the dissolu-

Table 2. Alloy-electrolyte interface parameters extracted from the EIS test

Alloy	Temperature (°C)	R_s (Ωcm^2)	R_p (Ωcm^2)	P×10^{-4} (F)	n	C_{ct} (μF.Cm^{-2})
304L	25	4	219	1.32	0.86	77.4
	40	3.8	110	1.01	0.81	34.3
	60	2.8	106	1.24	0.78	37.4
316L	25	5	376	0.72	0.90	53.3
	40	4.5	315	0.91	0.87	60.11
	60	3.5	144	1.20	0.81	56.0

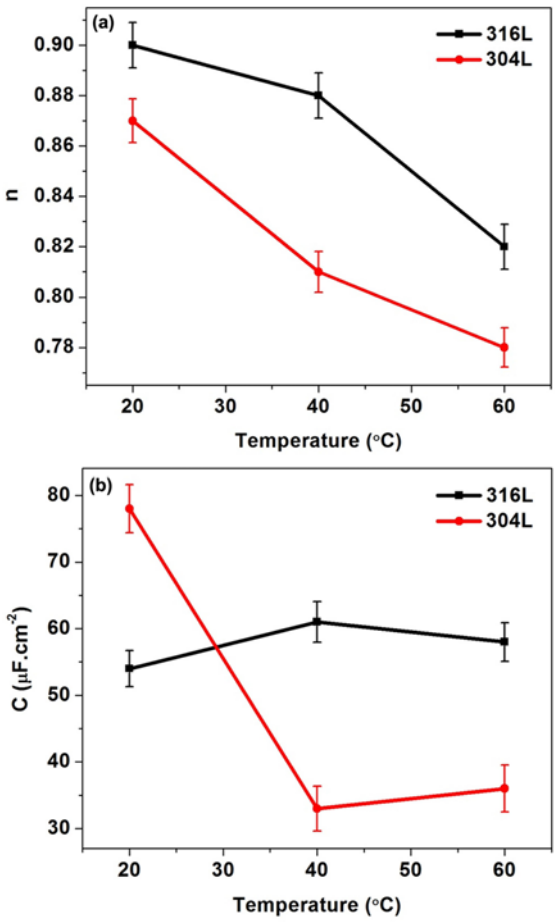

Fig. 4. (a) Alloy surface heterogeneity (n) and (b) charge transfer (C_{ct}) variations with temperature based on the EIS results.

tion in the 304L alloy creates a more uneven surface (about 7% at 40 °C) in comparison with the 316L alloy.

In the 304L alloy, by increasing the temperature to 40 °C, C_{ct} decreases rapidly from 77 to 34 μF and by further increases to 60 °C, it increases slightly to 37 μF. However, in the 316L alloy, the C_{ct} value increases slightly from 53 to 61 μF, and it reached 56 μF at 60 °C. It is well known that the capacitance is inversely proportional to the surface film thickness [36,41]:

$$C_{ct} = \frac{\varepsilon_o \varepsilon}{d} S \tag{3}$$

where d is the thickness of the charge transfer layer, S is the surface area of the alloy, ε_0 is the permittivity of the air, and ε is the local dielectric constant. A decrease in C_{ct} is an indication of the surface layer thickening.

The 304L alloy shows a significant decrease in C_{ct} when the temperature increases to 40 °C. Therefore, a thickening process could occur on the 304L alloy at this temperature range. Since the n value also decreases in this temperature range due to the uneven dissolution process, an irregular surface layer thickening of a more porous structure could be developed on the 304L alloy. At 60 °C, because the C value remains almost constant (Fig. 4(b)) and n continuously decreases (Fig. 4(a)), the surface layer thickness does not change significantly; however, the layer becomes significantly rougher.

In contrast, different processes occurred on the 316L alloy surface. Because C_{ct} remains almost constant, the surface layer thickness does not change significantly. However, considering a significant decrease in the n value (from 0.9 to 0.81) with the increase in temperature from 40 to 60 °C, the surface layer becomes more porous. The C and n variations also confirm the R_p values because the decrease in R_p from 40 to 60 °C is greater (from 330 to 150 Ω.cm^2) than that from 20 to 40 °C (from 430 to 330 Ω.cm^2).

In summary, the increase in temperature to 60 °C develops a rougher (3%) and thicker (34%) surface layer on the 304L alloy compared with those of the 316L alloy, where a relatively more uniform and compact surface layer was formed.

In order to confirm the obtained n values, the surface heterogeneity was characterized using high resolution SEM imaging. Figure 5 shows the SEM images of the rinsed and dried specimens after exposure to the 15 ppm H_2S solution. As an example, the attacked surface of the 304L alloy at 60 °C with the highest porosity (n = 0.78) was compared with the

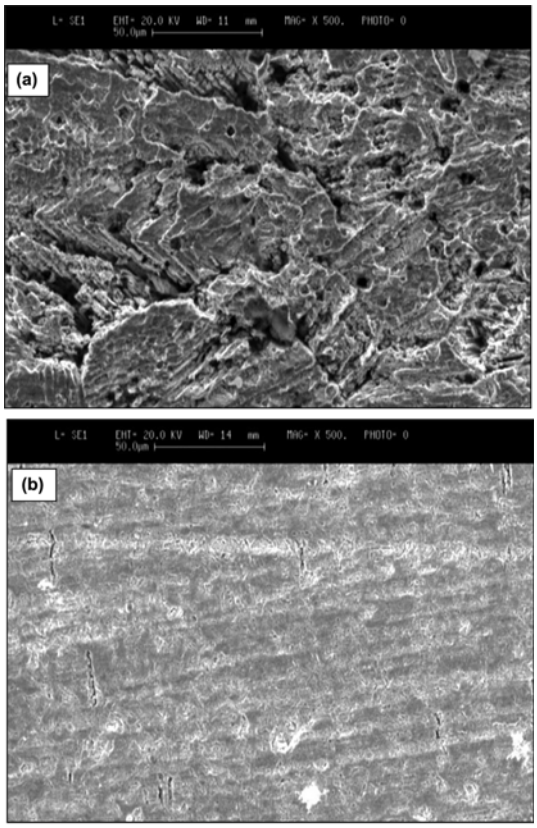

Fig. 5. SEM images of the attacked surface of (a) the 304L alloy at 60 °C with highest porosity (n = 0.78 from EIS test) and (b) 316L alloy at 25 °C with lowest porosity (n = 0.90 from EIS test) immersed in 15 ppm H_2S solution.

316L alloy at 25 °C with the lowest porosity ($n = 0.90$). Clearly, a general attack (without evidence of localized corrosion) was observed on both alloy surfaces. Furthermore, on the 304L alloy surface, the attacked surface was rougher and more heterogeneous than that of the 316L alloy, which confirms the n variations obtained via EIS in Fig. 4. The formation of the surface layer on the 316L alloy with less porosity is associated with the beneficial influence of the molybdenum alloying element [12]. Moreover, it appears that the thin layer with higher porosities formed on the 304L alloy leads to crack formation at the outmost alloy surface, which is clear in the SEM images.

Simultaneous C and n value comparisons verify that H_2S develops a rougher and thicker surface layer. Based on the above EIS (calculated n and C values) and SEM images, and to exemplify the alloy surface layer evolution, a sketch of the sample cross section was drawn. Figure 6 depicts a schematic view of the relative charge transfer layer thickness and its heterogeneity variations in the two alloys at corrosion potential conditions after exposure to 15 ppm H_2S containing media at different temperatures. For simplification, the initial air formed oxide layer (FeO-Cr_2O_3) is not shown. Moreover, the air formed oxide was almost dissolved in the present solution and replaced by a sulfide layer [3,12]. The scheme clearly demonstrates that at similar temperature conditions, a thicker and slightly more homogenous charge transfer layer is formed on the surface layer of the 316L alloy, and this is consistent with the SEM results in Fig. 5. This difference is more pronounced at 40 °C.

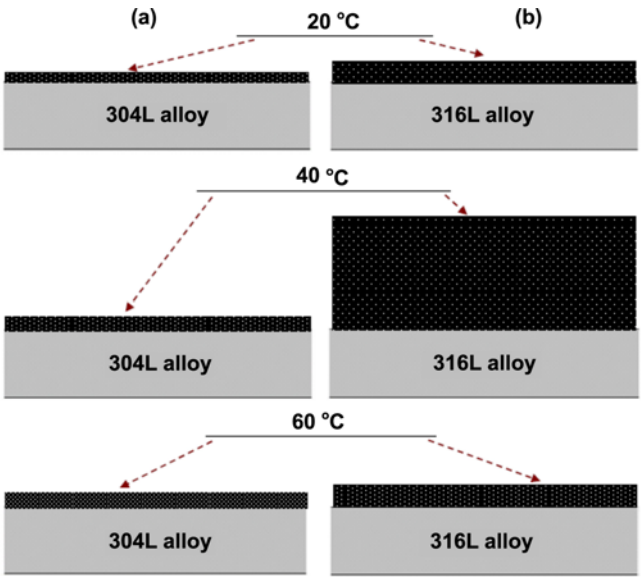

Fig. 6. Schematic images of the relative charge transfer layer thickness and its heterogeneity in the (a) 304L and (b) 316L alloys exposed to the 15 ppm (by mole) H_2S containing media at various temperatures. The white spots represent the heterogeneity of the charge transfer capacitance estimated from n variations. For simplicity, the initial air formed oxide layer ($FeCr_2O_4$) is not shown.

Compared with the previous results for H_2S corrosion [12], these results clarify that while both alloys increase in H_2S concentration does not significantly change the n value, increases in the temperature decrease the n value significantly (from 0.87 to 0.78 in the 304L alloy and from 0.9 to 0.81 in the 316L alloy). This indicates that the temperature has a greater influence on the n value, i.e. the surface roughness. In addition, the increase in H_2Sconcentration in both alloys led to a 50% increase in the C_{ct} value (i.e. the surface layer thickness decreases by approximately 50%). In contrast, with increases in the temperature, the C_{ct} value for the 304L alloy decreased by half (i.e. the surface layer thickness almost doubled) and in the 316L alloy, it remained almost unchanged (i.e. the surface layer thickness was more or less constant).

In summary, in the 316L alloy, the influence of the H_2S concentration was more profound than the temperature, which led to surface layer thinning [12]. This means that in the 316L alloy, the H_2S concentration functions as a kinetics parameter and facilitates the dissolution process in the dissolution formation. However, in the 304L alloy, although increases in the H_2S concentration have the same effect, i.e. cause the surface to be thinner [12], the increases in the temperature

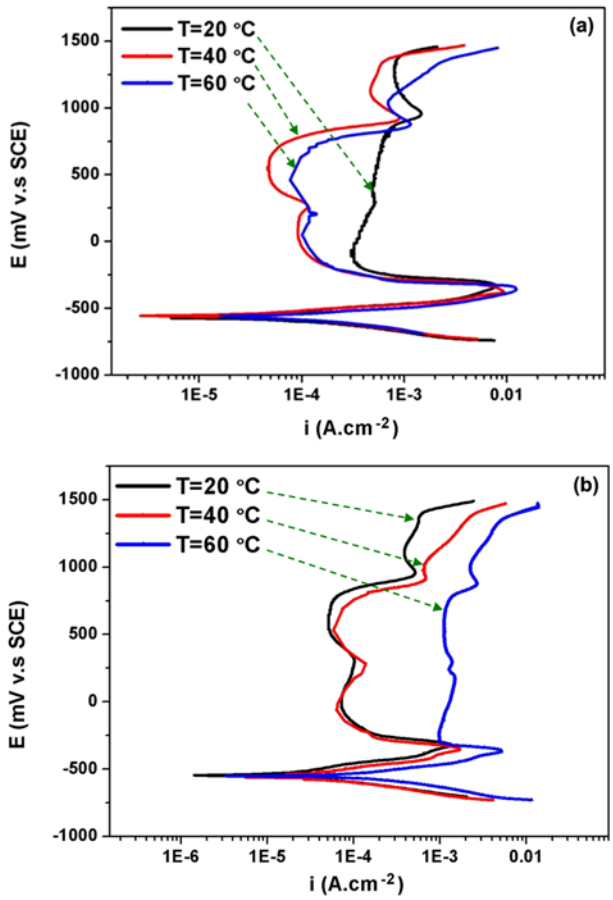

Fig. 7. Potentiodynamic polarization curves of the (a) 304L and (b) 316L alloys at various temperatures in the 15 ppm H_2S solution.

thicken the surface layer and kinetically promote surface layer formation in the dissolution formation.

3.4. Potentiodynamic polarization results

The PDP results are shown in Fig. 7. Four regions could be observed in the PDP curves at higher potentials: cathodic region, active anodic region, passive region, and transpassivity. In all conditions, the solutions were a sulfur-containing media in the presence or absence of H_2S; similar active-passive behaviors could be observed in both alloys in which the critical current density (i_{cr}) and passivation current density (i_p) could be obtained.

In addition to the proton ions from the acid base solution, H_2S also generated protons. The chemical reactions including the proton reduction are as follows [27,28]:

$$H_2S \rightarrow H^+ + HS^- \quad (4)$$
$$HS^- \rightarrow H^+ + S^{2-} \quad (5)$$
$$2H^+ + 2e^- \rightarrow H_2 \text{ or } 2H \quad (6)$$

Increases in the temperature accelerated the kinetics of the above reactions (Eqs. 4 to 6), and consequently the anodic dissolution. The Fe dissolution can be represented by the following reactions [32,33]:

$$Fe + H_2S + H_2O \rightarrow Fe(HS^-)_{abs} + H_3O^+ \quad (7)$$
$$(FeHS^-)_{ads} \rightarrow (FeSH^+)_{ads} + 2e^- \quad (8)$$
$$(FeSH^+)_{ads} + H3O^+ \rightarrow Fe^{2+} + H_2S + H_2O \quad (9)$$

In addition, sulfide ions can act as surface catalysts and speed up the anodic dissolution, which can be distinguished in the LPR and OCP results.

The i_{cr} and i_p values at a potential of 500 mV vs. SCE (for comparison) are plotted in Fig. 8. At low temperatures, the i_{cr} in the 316L alloy was smaller than that in the 304L alloy. Therefore, the passivation on the 316L alloy was easier than that on the 304L alloy. With increases in temperatures, the i_{cr} increased in both alloys. This indicates that the temperature accelerates the dissolution process and impedes the formation and growth of the passive layer on both alloys. However, the influence of the temperature on hindering the passivation on the 316L alloy was larger than that on the 304L alloy. This can be verified by the increase in temperature to 60 °C resulting in the i_{cr} in the 316L alloy increasing by approximately five times, whereas in the 304L alloy, it only increased by 1.5 times with respect to the corresponding temperature values.

Interestingly, the passivation current density (i_p) variations exhibited different behaviors in the two alloys. With the increase in temperature to 40 °C, the i_p of the 304L alloy decreased significantly, by one decay, and increased two-fold to 0.12 mA.cm^{-2} when the temperature increased to 60 °C. In the 316L alloy, with the increase in temperature to 40 °C, i_p increased three times, and with a further increase in temperature to 60 °C, it increased again by approximately one decay, reaching 1.1 mA.cm^{-2}. This indicates that while the i_p in the 316L alloy was smaller than that of the 304L alloy at a low temperature, in a high temperature region, the i_p of the 316L alloy increases more than that of the 304L alloy. It appears that increases in temperature could create more favorable conditions for sulfide surface layer formation on the 304L alloy, particularly at 40 °C. In contrast, the temperature increase led to difficulty in the passive layer maintenance in the 316L alloy compared with in the 304L alloy.

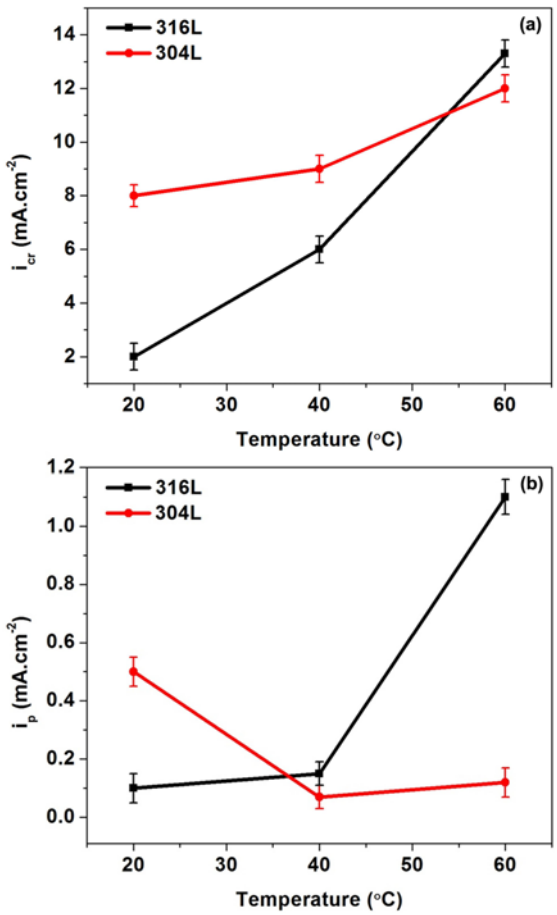

Fig. 8. (a) Critical passivation current density (i_{cr}) and (b) passivation current density (i_p) at potential 500 mV vs. SCE of the 304L and 316L alloys in the 15 ppm H_2S solution at various temperatures.

The absolute values of i_{cr} and i_p, and the i_{cr}/i_p ratio could also provide a general idea for comparison between the passivation tendencies of the two alloys. As seen in Figs. 8(a) and 8(b), for the 304L alloy, the temperature 40 °C provides the highest i_{cr}/i_p ratio, which was approximately 154:1. Even at a temperature of 60 °C, this ratio was approximately 100:1. In contrast, in the 316L alloy, the highest i_{cr}/i_p ratio could be obtained at room temperature (20 °C) and with temperature increases to 60 °C, this ratio decreased to 12:1. Therefore, it can be concluded that the increase in temperature has a negative effect on the passivation of the 316L alloy and a relatively constructive effect on the 304L alloy passivation (particularly at 40 °C).

In summary, for both alloys, increases in either the H_2S concentration or temperature significantly increase the i_{cr} value in which it is more profound in the 316L alloy, which indicates an analogous harmful effect of these two kinetic parameters on passivation [12]. However, the i_p on the 316L alloy increased with increases in either temperature or H_2S concentration, in contrast to the i_p of the 304L alloy decreasing with increases in either the temperature or H_2S concentration. This indicates that in the 304L alloy, increases in temperature and/or H_2S concentration create more favorable conditions for passivation stability by kinetically promoting the surface layer formation in dissolution formation [12].

The difference in the corrosion behaviors of the 304L and 316L alloys at various temperatures can be related to the chemical reactions involving the alloying elements Cr, Ni, and Mo.

3.5. Pourbaix diagrams

A previous study revealed that the active and passive behaviors of the two alloys could also be investigated in more detail using multi-component Pourbaix diagrams [12]. According to the Pourbaix diagram in Fig. 9, in the present study, the passivation of the 304L alloy could be associated with the surface layer containing the M_2O_3 oxide (M is Fe and Cr). With increases in the temperature, the formation of FeS_2 in the passivation region could assist the passive layer integrity as in the following reaction:

$$Fe + 2H_2S \rightarrow FeS_2 + 2H_2 \quad (10)$$

The presence of FeS_2 could be predicted from thermodynamic calculations, as seen in Fig. 9. By detaching the iron sulphide species from the surface at sufficiently high potential, FeS_2 is dissolved and iron hydroxide compounds are formed.

Based on the Pourbaix diagrams, nickel does not contribute to the passive layer at pH 3andisdissolved accordingly [12,40]. Moreover, chromium does not have an affinity to react with H_2S, [42], and it presents at the passive layer in oxide form, i.e. M_2O_3 (M is Fe and Cr).

The passivation of the 316L alloy at a lower potential region was also similar to that of the 304L alloy. However, in addition to FeS_2, Mo could also participate in the surface passive layer as MoS_2 and MoO_2, as shown in Fig. 10. The following general reactions are proposed for Mo [3]:

$$Mo + 2H_2S \rightarrow MoS_2 + 2H_2 \quad (11)$$
$$Mo + 2H_2O \rightarrow MoO_2 + 2H_2 \quad (12)$$

In summary, the better corrosion resistance of the 316L alloy at the free potential, OCP, LPR, and EIS conditions could be exclusively associated with its Mo content and formation of sufficient MoS_2 and MoO_2 compounds. Research performed on the individual alloying elements of Cr, Ni, and Mo in media containing sulphur species and H_2S revealed greater corrosion resistance of the Mo element compared with the other two alloying elements, Cr and Ni. In both

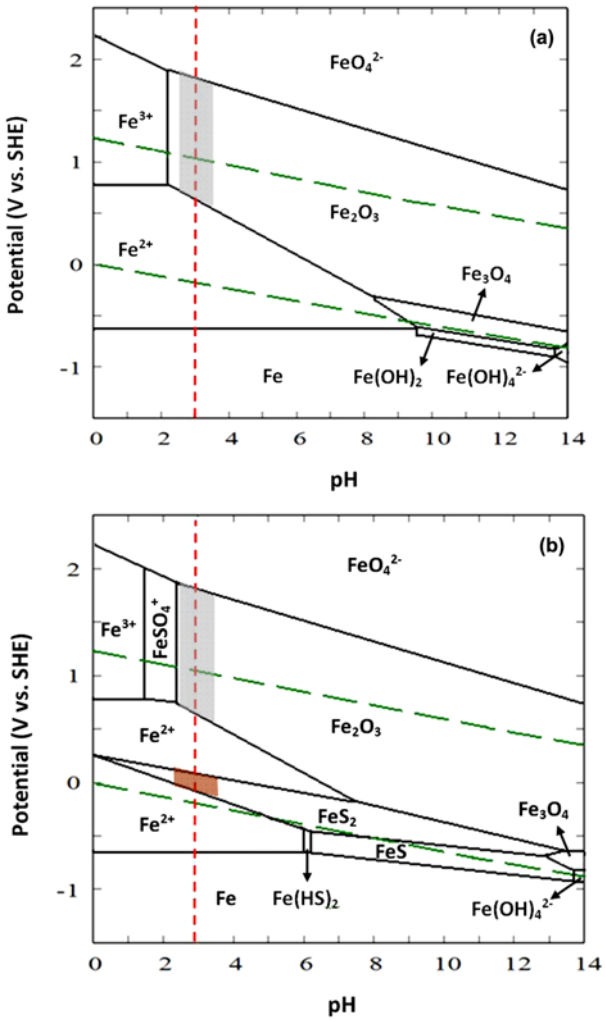

Fig. 9. Satiability (Pourbaix) diagrams of the (a) Fe-H_2O and (b) Fe-H_2O-S systems at the 15 ppm (by mole) H_2S concentration (T = 60 °C; $[Fe^{2+}(aq)] = 10^{-6}$ M).

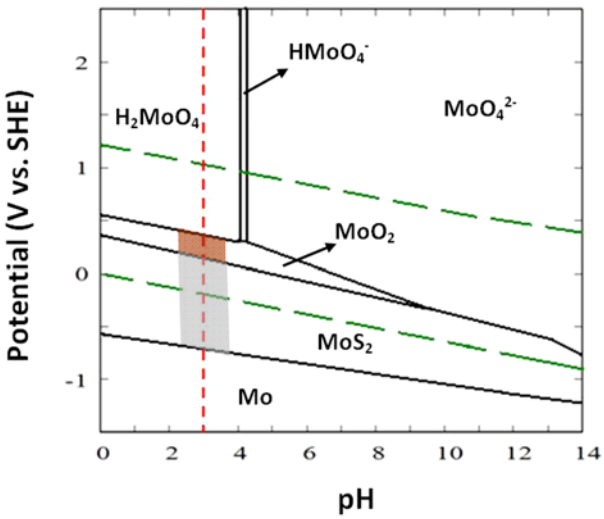

Fig. 10. Stability (Pourbaix) diagrams of the Mo-H_2O-S systems at 15 ppm (by mole) H_2S concentration (T = 60 °C; $[Mo^{4+}(aq)] = 10^{-6}$ M).

alloys in acidic media, the alloy surfaces were covered by HS^- and S^{2-}. In the 304L alloy, thermodynamically, Fe tends to form sulfide compounds (FeS_2), which somehow assist the protective surface layer. However, at the low potential region in the 316L alloy, MoS_2 and MoO_2 contributed to the passivation improvement as seen in the EIS and PD results presented in Figs. 3(b) and 7(b), respectively.

In order to verify the presence of various sulfide compounds predicted by the Pourbaix diagrams, XRD measurements were taken and the results are shown in Fig. 11. Despite the sample surface changing during the *ex-situ* XRD characterization, it confirmed the presence of iron sulfides (FeS_2 and FeS) on the 304L alloy and both iron sulfides (FeS_2 and FeS) and molybdenum sulfide (MoS_2) on the 316L alloy [12].

It should be noted that in addition to the temperature fluctuations, the pH variations that are inevitable in most industrial applications and have a crucial effect on the passivation behavior can be seen in the Pourbaix diagrams [40]. This is an important issue because during application, e.g. gas purification processes, increases in the pH could change the situation in the region where chromium oxide can be formed and significantly assist the passivation.

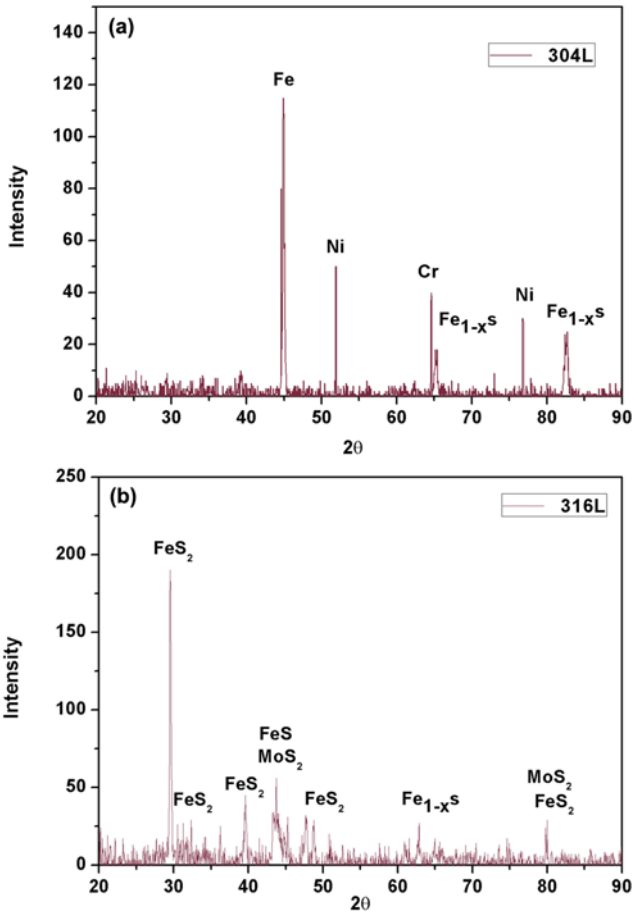

Fig. 11. XRD results for the (a) 304L and (b) 316L alloys exposed to 15 ppm H_2S containing media at 40 °C.

It is also interesting to investigate the H_2S corrosion at higher H_2S concentrations [2,14].This would be very useful because it can occur in some sour gas refining process units and the kinetics of surface layer dissolution formation may change significantly with the presence of large amounts of H_2S.

Due to the greater corrosion resistance at the free potential exposure, it appears that the 316L alloy is a better candidate in the present investigated temperature range. However, in the passivity region, with increases in temperature, the passivation current density in the 304L alloy is noticeably lower than that in the 316L alloy, which means that its maintenance is less expensive. In particular, at a temperature of 40 °C and concentration of 15 ppm H_2S, the passivation in the 304L alloy is significantly greater than that of the 316L alloy.

4. CONCLUSIONS

In this study, the corrosion of 304L and 316L stainless steels in 15 ppm laboratory-based H_2S produced by Na_2S in an oxygen-free H_2SO_4 + Na_2SO_4 solution at pH 3 was investigated at three temperatures: 20, 40 and 60 °C. The results can be summarized as follows.

(1) The OCP, LPR, and EIS results exhibited similar trends in corrosion for the two alloys, but a slightly lower corrosion rate was observed for the 316L alloy. The charge transfer mechanisms were determined on both alloy-electrolyte interfaces with a single capacitive loop containing the CPE element. With increases in the temperature to 60 °C, the corrosion resistance of both alloys decreased.

(2) The *n* and *C* variations revealed that a distinct corrosion behavior could be observed in the temperature range from 20 to 40 °C and from 40 to 60 °C for the two alloys. While the formation of a thicker and more porous layer on the 304L alloy occurred in the 20 to 40 °C range, the surface roughness on the 316L alloy primarily increased in the 40 to 60 °C range. The *C* and *n* variations also confirmed the polarization resistance (R_p) values obtained for both alloys.

(3) The absolute values of the critical and passivation current densities and their ratio in the potentiodynamic polarization results revealed that temperature increases had a negative effect on the passivation of the 316L alloy and had a relatively constructive effect on the 304L alloy passivation (particularly at 40 °C).

(4) The multi-component Pourbiax diagrams of the constituent alloying elements revealed that in the 304L alloy, the surface layer composition was most likely FeS_2, but in the 316L alloy, its composition was primarily FeS_2 and MoS_2. The formation of iron and molybdenum sulfur compounds was verified through XRD analyses.

(5) Increases in the temperature kinetically provided more favorable conditions for the FeS_2 formation than the MoS_2 formation. This was verified via the lower passivation current

density in the 304L alloy at higher temperatures.

(6) Due to its greater corrosion resistance at the free potential condition, the 316L alloy is a better candidate in the present investigated temperature range. However, in the passivity region, with increases in the temperature, the passivation current density on the 304L alloy was noticeably lower than that of the 316L alloy, which indicates that its maintenance is less expensive. In particular, at 40 °C and 15 ppm H_2S, the passivation on the 304L alloy was significantly greater than that in the 316L alloy.

ACKNOWLEDGMENTS

The authors would like to thank Mojtaba Momeni and Reza Parvizi for their valuable assistance and discussions. Also, Shiraz University and Hakim Sabzevari University are acknowledged for providing experimental facilities and financial support.

REFERENCES

1. L. Smith, B. Nisbet, and E. Wade, *Corrosion Resistant Alloys for Oil and Gas Production: Guidance on General Requirements and Test Methods for H_2S*, pp.1-19, European Federation of Corrosion Publications, No. 17. 2nd ed., Maney Materials Science, London (2002).
2. A. L. Kohl and R. Nielsen, *Gas Purification*, 5th ed., Gulf Publishing Company, Houston, Texas (1997).
3. P. Marcus, *Corrosion Mechanisms in Theory and Practice* 3rd ed., CRC Press, Amsterdam (2011).
4. J. Aali, H. Rahimpour-Bonab, and M. R. Kamali, *J. Petrol. Sci. Eng*. **50**, 161 (2006).
5. Y. Shirvany, G. Zahedi, and M. Bashiri, *J. Petrol. Sci. Eng*. **73**, 156 (2010).
6. K. Mahdi, R. Gheshlaghi, G. Zahedi, and A. Lohi, *J. Petrol. Sci. Eng*. **61**, 116 (2008).
7. G. Zhu, S. Zhang, H. Huang, Q. Liu, Z. Yang, J. Zhang, T. Wu and Y. Huang, *J. Petrol. Sci. Eng*. **71**, 30 (2010).
8. M. S. H. Bader, *Desalin*. **201**, 121 (2006).
9. M. S. H. Bader, *J. Petrol. Sci. Eng*. **55**, 93 (2007).
10. J. Klein, M. van Afferden, F. Pfeifer, and S. Schacht, *Fuel Process. Tech*. **40**, 297 (1994).
11. A. L. Kohl and R. B. Nielsen, *Liquid Phase Oxidation Processes for Hydrogen Sulfide Removal. Gas Purification*, 5th ed. pp.731-865, Gulf Professional Publishing, Houston, Texas (1997).
12. A. Davoodi, M. Pakshir, M. Babaiee, and G. R. Ebrahimi, *Corros. Sci*. **43**, 399 (2011).
13. C. C. Silva, J. P. S. E. Machado, A. V. C. Sobral-Santiago, H. B. de Sant'Ana, and J. P. Farias, *J. Petrol. Sci. Eng.* **59**, 219 (2007).
14. J. J. Carroll, *Proc. 1st Annual Gas Processing Symp.*(eds. E. A. Hassan, G. V. R. Reklaitis, and M. E. H. Mahmoud), p.276, Elsevier, Amsterdam (2009).
15. K. L. Ding, S. Y. Li, C. T. Yue, and N. N. Zhong, *J. Fuel Chem. Tech*. **35**, 401(2007).
16. M. Mohsen-Nia, H. Moddaress, and G. A. Mansoori, *J. Petrol. Sci. Eng*. **12**, 127(1994).
17. P. Mougin, V. Lamoureux-Var, A. Bariteau, and A. Y. Huc, *J. Petrol. Sci. Eng*. **58**, 413 (2007).
18. M. S. H. Bader, *Desalin*. **201**, 100 (2006).
19. M. El-Said, M. Ramzi, and T. Abdel-Moghny, *Desalin*. **249**, 748 (2009).
20. H. R. Khatami, M. Ranjbar, M. Schaffie, and M. A. Emady, *J. Petrol. Sci. Eng*. **71**, 13 (2010).
21. X. Liu, L. Jungang, Z. Qianya, F. Jinlai, L. Yingli, and S. Jingxin, *J. Petrol. Sci. Eng*. **66**, 161 (2009).
22. M. Salman, H. Qabazard, and M. Moshfeghian, *J. Petrol. Sci. Eng*. **55**, 48 (2007).
23. X. M. Dong, Q. C. Tian, and Q. A. Zhang, *Corros. Eng. Sci. Tech*. **45**, 181 (2010).
24. O. Karpash, I. Darvay, and M. Karpash, *J. Petrol. Sci. Eng*. **71**, 133 (2010).
25. S. Eliassen and L. Smith, *Guidelines on Materials Requirements for Carbon and Low Alloy Steels for H_2S-Containing Environments in Oil and Gas Production*, European Federation of Corrosion Publications, No. 16, 3rd ed., Maney Materials Science, London (2009).
26. S. Nesic, *Corros. Sci*. **49**, 4308 (2007).
27. H. H. Huang, J. T. Lee, and W. T. Tsai, *Mater. Chem. Phys*. **58**, 177 (1999).
28. C. Ren, D. Liu, Z. Bai, and T. Li, *Mater. Chem. Phys*. **93**, 305 (2005).
29. W. Sun and S. Nesic, *NACE proceedings*, Paper No. 066442006 (2006).
30. W. Sun and S. Nesic, *NACE proceedings*, Paper No. 076552007 (2007).
31. K. L. J. Lee and S. Nesic, *NACE proceedings*, Paper No. 056302005 (2005).
32. H. Ma, X. Cheng, S. Chen, C. Wang, J. Zhang, and H. Yang, *J. Electroanal.Chem*. **451**, 11 (1998).
33. H. Ma, X. Cheng, G. Li, S. Chen, Z. Quan, S. Zhao, and L. Niu, *Corros. Sci*. **42**, 1669 (2000).
34. Z. F. Yin, W. Z. Zhao, W. Y. Lai, and X. H. Zhao, *Corros. Sci*. **51**, 1702 (2009).
35. S. J. Yuan and S. O. Pehkonen, *Corros. Sci*. **49**, 1276 (2007).
36. M. E. Orazem and B. Tribollet, *Electrochemical Impedance Spectroscopy*, John Wiley & Sons, Inc. New York (2008).
37. X. Cheng, H. Ma, S. Chen, X. Chen, and Z. Yao, *Corros. Sci*. **42**, 299 (2000).
38. X. Cheng, H. Ma, S. Chen, L. Niu, S. Lei, R. Yu, and Z. Yao, *Corros. Sci*. **41**, 773 (1999).
39. I. Puigdomenech, Medusa, *Chemical Equilibrium Diagrams. Stockholm*: Royal Institute of Technology, Department of Chemistry, Stockholm, Sweden (2010).
40. B. Beverskog and I. Puigdomenech, *Corrosion* **55**, 1077 (1999).
41. B. Hirschorna, B. Tribollet, V. Vivier, I. Frateur, and M. Musiani, *Electrochem.Acta* **55**, 6218 (2010).
42. T. Chevreau, D. Cornet, M. Marzin, and K. Roudias, *Mater. Chem. Phys*. **26**, 269(1990).